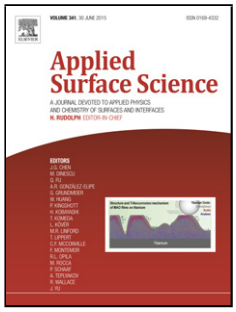

Title: Facile synthesis of $CoNi_2S_4/Co_9S_8$ composites as advanced electrode materials for supercapacitors

Authors: Fenglin Zhao, Wanxia Huang, Hongtao Zhang, Dengmei Zhou

PII: S0169-4332(17)32056-1
DOI: http://dx.doi.org/doi:10.1016/j.apsusc.2017.07.066
Reference: APSUSC 36600

To appear in: *APSUSC*

Received date: 11-5-2017
Revised date: 5-7-2017
Accepted date: 8-7-2017

Please cite this article as: Fenglin Zhao, Wanxia Huang, Hongtao Zhang, Dengmei Zhou, Facile synthesis of CoNi2S4/Co9S8 composites as advanced electrode materials for supercapacitors, Applied Surface Sciencehttp://dx.doi.org/10.1016/j.apsusc.2017.07.066

Facile synthesis of $CoNi_2S_4/Co_9S_8$ composites as advanced electrode materials for supercapacitors

Fenglin Zhao[a], Wanxia Huang[a,*], Hongtao Zhang[b] Dengmei Zhou[a],

[a] College of Materials Science and Engineering, Sichuan University, Chengdu 610065, China

[b] Department of Materials, Loughborough University, Leicester LE11 3TU, UK

[*] Corresponding authors. E-mail: huangwanxia@scu.edu.cn

Highlights

- 1. $CoNi_2S_4/Co_9S_8$ composites were firstly synthesized by chemical bath deposition.
- 2. Large specific surface area and special 3D architecture benefit electrochemical performance.
- 3. $CoNi_2S_4/Co_9S_8$ composites delivered high specific capacitance of 1183.3 Fg^{-1} at 2 Ag^{-1}.
- 4. $CoNi_2S_4/Co_9S_8$ composites exhibited outstanding capacitance retention of 97.3% after 1000 cycles.

Abstract

In this paper, a facile chemical bath deposition method was utilized to synthesize three-dimensional nanostructured $CoNi_2S_4/Co_9S_8$ (CNSCS) composites as advanced electrode materials for high performance supercapacitors. CNSCS composites showed remarkable electrochemical performance owing to the high porosity, appropriate pore size distribution, novel architecture and synergistic effect of Ni/Co ions. The electrochemical tests revealed that CNSCS composites exhibited high specific capacitance (1183.3 Fg^{-1} at the current density of 2 Ag^{-1}), excellent rate performance (74.9% retention with tenfold current density increase) and outstanding cycle life stability. Moreover, the effect of temperature on electrochemical performance of CNSCS composites was investigated and the results indicated the specific capacitance of $CoNi_2S_4/Co_9S_8$ can keep relatively stable in a wide temperature from 0°C to 50°C. These results indicated that the synthesized CNSCS composites can be a promising electrode materials candidate for supercapacitors and chemical bath deposition is a promising processing route for CNSCS composites production.

Keywords: $CoNi_2S_4/Co_9S_8$ composites; Chemical bath deposition; Supercapacitors; Electrode materials; Three-dimensional architecture

1. Introduction

The reduced availability of fossil fuels and the soaring levels of air pollution require the development of the renewable and sustainable energy storage devices [1-3]. As a bridge of traditional electrostatic capacitors and rechargeable batteries, supercapacitors (also called electrochemical capacitors) have been considered as one of the most promising energy conversion and storage systems in virtue of their advantages of fast charge/discharge rate, long cycling lifetime, and ultrahigh power density [4-6]. It is believed that supercapacitors show huge promising applications in the field of electric vehicles, regenerative braking systems, uninterruptible power supplies and portable electronics [5, 7]. According to intrinsic energy storage mechanism, supercapacitors can be divided into electric double layer capacitors (EDLCs) and pseudocapacitors [8-9]. The capacitance of EDLCs relies on the physical absorption/desorption of electrostatic charges from the surface of active materials, but pseudocapacitors can exhibit much higher specific capacitance through reversible Faradic reaction between electrode materials and electrolytes [8, 10-13].

Generally speaking, the performance of supercapacitors intensely relies on the property of electrode materials. Carbon-based materials have been predominantly used for EDLCs, such as mesoporous carbon, activated carbon, carbon aerogel, carbon nanotubes and graphene [14].Transition metals oxides (such as MnO_2, NiO, Co_3O_4, RuO_2), chalcogenides (Co_9S_8, Ni_3S_2, etc), hydroxides [$Co(OH)_2$, $Ni(OH)_2$, etc] and conducting polymers (polypyrrole, polyaniline, etc) have been intensively studied as electrode materials for pseudocapacitors [10, 15-17]. Among them, ternary nickel cobaltite sulfide ($NiCo_2S_4$ or $CoNi_2S_4$, denoted as NCS) have been recognized as one of the most promising candidates for electrode materials due to some special characters, such as high electrical conductivity, high electrochemical activity, environmental friendliness and low cost [18, 19]. Up to now, NCS have been investigated for potential applications in the field of lithium-ion batteries [20],

catalysts [21] and supercapacitors [15]. NCS with different nanostructures, such as nanowires [22], hexagonal nanoplates [23], urchin-like [18], nanosheets [24], and hollow microsphere [25] are particularly attractive for the application of supercapacitors. However, fabrication of NCS with a facile and scalable processing route is still challenging.

Hydrothermal (or solvothermal) method has been largely adopted for the synthesis of NCS at present. For example, Zhao *et al*. [26] synthesized cross-linked $CoNi_2S_4$ on SiC supporters by hydrothermal technology, and the $CoNi_2S_4$ showed high specific capacity (231.1 mAh/g at 2 A/g) and outstanding rate capability. Shen *et al*. [27] used a hydrothermal method to prepare $CoNi_2S_4$/CNT/graphene composites which had high specific capacitance (710 F/g at 20 A/g) and the capacity retained 82% after 2000 charging-discharging cycles. Li *et al*. [28] reported a solvothermal method to synthesize $NiCo_2S_4$ which had high specific capacitance of 1304 F/g at 2 A/g, excellent rate capability of 1116 F/g at 20 A/g. However, the disadvantages of the hydrothermal method such as long reaction time, high reaction pressure/temperature, and low production level greatly hinder large-scale production of NCS [29]. Hence, it is urgent to develop a facile and cost-effective method to synthetize transition metal sulfide. The chemical bath deposition method was traditionally regarded as an effective strategy to prepare films. For example, Karade *et al*. [30] developed MoS_2 thin films by room temperature chemical bath deposition method. Hu *et al*. [31] fabricated MnO_2 thin films on ITO/PET substrates by chemical bath deposition. So it will be a challenging and interesting to synthesize ternary nickel cobaltite sulfide powders by chemical bath deposition method. Besides, Co_9S_8 served as another hopeful electrode materials because of its high specific capacitance draw much attention, but its cycle performance hinder its development [32-33]. Thus, the fabrication of $CoNi_2S_4$/Co_9S_8 (denoted as CNSCS) composites may be a desirable method to acquire comprehensively high-performance supercapacitors electrode materials.

In this paper, we proposed a facile chemical bath deposition method to fabricate CNSCS composites as high-performance supercapacitors electrode materials. Combined with large specific surface area, appropriate pore size distribution and novel architecture, CNSCS composites exhibited high specific capacitance, excellent rate performance and outstanding cycling stability. Moreover, the effect of temperature on CNSCS's electrochemical performance indicated CNSCS can keep relatively stable in a wide temperature range.

2. Experimental

2.1 Materials and synthesis

In the preparation of CNSCS composites, 1.164 g $Ni(NO_3)_2 \cdot 6H_2O$, 2.328 g $Co(NO_3)_2 \cdot 6H_2O$, 2.243 g hexamethylenetetramine were dissolved in deionized water (50 mL) and ethanol (20 mL) with continuous magnetically stirring for 20 min. Then the mixed solution was refluxed in an oil bath at 150 °C for 2 h. The precipitates were collected from the solution and washed several times with deionized water and ethanol by centrifugation. 0.2 g thioacetamide and above centrifugation products were dissolved in 70 mL deionized water and stirred for 30 min. The mixed solution was again refluxed in an oil bath at 130 °C for 3 h. The products were collected and washed three times with deionized water and ethanol by centrifugation. Finally, above products were dried in a vacuum oven at 60 °C for 12 h. For comparison, $CoNi_2S_4$ was prepared by similar synthetic process except the weight of TAA changed to 0.5g.

2.2 Characterizations

The crystal structure of the samples were characterized by X-ray diffraction (XRD, Bruker D8 Advance) using Cu K_α (λ=0.15418 nm) radiation in the range of 10°-80° with a step of 0.02°. X-ray photoelectron spectroscopy (XPS, Thermo ESCALAB 250XI) measurement was carried out on Al K_α source (hv=1486.6 eV). The morphology and microstructure of the samples were directly examined by high resolution transmission electron microscopy (HRTEM, FEI Tecnai G20) and field emission scanning electron microscopy (FESEM, Hitachi S-4800). The Brunauer-

Emmett-Teller (BET) specific surface area and Barrett-Joyner-Halenda (BJH) pore size distribution of the samples were measured by nitrogen adsorption-desorption isotherms (Quadrasorb evo, Quantachrome Instruments) at 77 K.

2.3 Electrochemical measurements

The electrochemical properties of CNSCS composites were evaluated by a conventional three electrode system using electrochemical workstation (CHI660E, Shanghai Chenhua). The working electrode was prepared by mixing active material, acetylene black, polyvinylidene difluoride binder at a weight ratio of 8:1:1 with Nmethyl-pyrrolidone. The prepared slurry was firstly coated onto the nickel foam and then dried at 60 °C for 12 h in a vacuum oven. Then the nickel foam was pressed under a pressure of 10 MPa for 10 s. Platinum foil (15×15 mm) and Ag/AgCl (sat. KCl) were used as counter and reference electrode, respectively. 3M KOH was used as aqueous electrolyte. The different temperature tests were conducted at water bath kettle.

3. Results and discussion

Figure 1 is XRD pattern of powder produced by chemical bath deposition. The diffraction peaks at 26.72°, 31.32°, 38.16°, 50.10° and 54.92°can all be well indexed to the (220), (311), (400), (511) and (440) planes of the cubic $CoNi_2S_4$ phase (JCPDS 24-0334), respectively. In addition, the diffraction peaks at 15.32°, 29.92°, 47.34° and 53.04° correspond to the (111), (311), (511) and (440) planes of Co_9S_8 phase (JCPDS 86-2273), respectively. Overall, the diffraction peaks of $CoNi_2S_4$ are much stronger than Co_9S_8, which indicates the as-prepared products are mainly composed of $CoNi_2S_4$ and combined with a small amount of Co_9S_8. So the samples we prepared can be assigned to the composites of $CoNi_2S_4/Co_9S_8$. For comparison, the $CoNi_2S_4$ was synthesized and its XRD pattern is shown in Fig. S1.

The surface composition and valence of the CNSCS composites were further tested by XPS, and the corresponding results are presented in Fig. 2. As shown in Fig. 2a, the composites are mainly composed of Ni, Co and S element. The Ni 2p, Co 2p, S 2p

spectra were individually fitted by Gaussian method in terms of spin-orbit doublets and shake-up satellites (marked as "Sat"). In Fig. 2b, Ni 2p spectrum can be fitted with two spin-orbit doublets and two shake-up satellites. As for Ni 2p spectrum, the binding energies situated at around 853.2 and 872.5 eV of the first doublet correspond to Ni^{2+} and those at around 855.8 and 873.5 eV of the second doublet correspond to Ni^{3+} [34-36]. Regarding to Co 2p spectrum(Fig. 2c), the fitted peaks at around 778.4 and 793.5 eV of the first doublet are ascribed to Co^{3+} and those at around 781.2 and 796.8 eV of the second doublet correspond to the spin-orbit characteristics of the Co^{2+} [34-36]. S 2p spectrum can also be fitted with two peaks and one shake-up satellite, as shown in Fig. 2d. The binding energy at around 161.7 eV (S $2p_{3/2}$) is attributed to the low coordination of sulfur ions on surface. The component at 162.7 eV (S $2p_{3/2}$) is ascribed to distinctive metal-sulfur bond [37]. According to above XPS analysis, we can conclude that the composites contain Co^{2+}, Co^{3+}, Ni^{2+}, Ni^{3+} and S^{2-}, which agree well with CNSCS composites. The abundant valence states can be ascribed to the fact that the valence states of composite powder around surface are much less stable than those of powder at inner region. Moreover, the coexistence of Co^{2+}, Co^{3+}, Ni^{2+} and Ni^{3+} cations is favorable for rich redox actions.

Fig. 3 shows the morphologies and microstructural features of CNSCS composites. As shown in Fig. 3a, the composites were mainly composed of three-dimensional (3D) tremella-like nanosheet and many tiny particles, which were anchored on the surface of nanosheet. The lateral size of nanosheet was 2~5 μm. The magnified image gives more details about the composites. Fig. 3b shows that the diameter of the particles is less than 100 nm and they homogeneously distribute on the surface of the sheet. And the special hierarchical nanostructure is in favor of large specific surface area. TEM images of composite powder are shown in Fig. 3c~e. The nanosheets are corrugated, which can greatly enhance their electrochemical rate capability [38]. The nanosheet was almost transparent with the thickness of less than 20 nm. Fig 3e shows the lattice fringes with an interplanar spacing distance of 0.284 nm, corresponding to the (311) lattice plane of the $CoNi_2S_4$ nanosheet.

To investigate the porous structure of the sample, the specific surface area and pore size distribution of CNSCS composites were investigated by nitrogen adsorption-desorption analysis and the results are shown in Fig. 4. As shown in Fig 4a, the nitrogen adsorption-desorption isotherm belongs to Langmuir H4 type isotherm that has an obvious hysteresis loop in the range of 0.6-1 relative pressure, which indicates the mesoporous characteristic of the sample [39]. The BET specific surface area of the sample is calculated to be 57.9 m^2/g, which is larger than most of the reported values [35, 39-40, 42]. The pore size distribution estimated by BJH method mainly distributes in the range of 1~4 nm and centered at 2.5 nm, suggesting its large specific surface area. The mesoporous structure combined with large specific surface area is quite advantageous to endow ample electroactive sites and shorten the charge/ion transport path which is extremely beneficial for Faradaic redox reaction.

The electrochemical properties of CNSCS composites were tested by cyclic voltammetry (CV), galvanostatic charge/discharge (GCD). Fig. 5a shows CV curves of the CNSCS composites in a voltage window of 0-0.6V at different scan rates of 2, 5, 10, 15, 20 mVs^{-1}. All the CV curves clearly displayed a pair of redox peaks, which demonstrate their typical pseudocapacitive behavior. As the scan rate increased up to 20 mVs^{-1}, the shape of CV curve was still well-retained, which implies excellent rate capability. Data analysis of CV curves at different scan rates indicated that anodic peak current is linearly proportional with the square root of the scan rate (Fig. 5b), which satisfies the equation $I=av^b$ (where I is current, v is the scan rate, a and b are adjustable parameter). Here b is just 0.5, which means the redox reactions are limited by semi-infinite diffusion [41].

According to the CV curves, the specific capacitance C_m (Fg^{-1}) can be calculated based on the following formula [5]:

$$C_m = \frac{1}{2mv(V_a - V_b)} \int_{V_a}^{V_b} I(V)dV$$

Where I(V) is the current (A), m is the mass of the active material (g), v is the scan rate (V/s), V_a is the initial potential (V), V_b is the terminate potential (V). In addition,

as shown in Fig 5c, the specific capacitance of CNSCS composites were calculated to be 1029.2, 971.7, 910.8, 857.2, and 804.6 Fg^{-1} at 2, 5, 10, 15 and 20 mVs^{-1}, respectively. Capacitance preservation remains ca. 78.2% at a high scan rate of 20 mVs^{-1}. The specific capacitance decreased with the increasing scan rate, which indicated slow kinetic reaction between active materials and electrolytes at higher scan rate.

In Fig. 6a, GCD measurements were performed to calculate the specific capacitance of CNSCS composites at various current densities ranging from 2 to 20 Ag^{-1}. The pseudocapacitive characteristic was once again confirmed by the obvious charge and discharge plateaus. The specific capacitance C_m (Fg^{-1}) can be calculated from the charge-discharge curves according to the following formula [15]:

$$C_m = \frac{I\Delta t}{m\Delta V}$$

Where I (A) is the applied discharge current, Δt (s) is the discharge time, m (g) is the mass of the active material, ΔV (V) is the discharge potential range. It can be observed that the specific capacitance of CNSCS composites can be calculated to be 1183.3, 1141.8, 1101.3, 1056.1, 1030.4, 1010.4, 963.0, 918.0, and 886.1 Fg^{-1} at the current densities of 2, 4, 6, 8, 10, 12, 15, 18 and 20 Ag^{-1}, respectively (as shown in Fig. 6b). The specific capacitance deceased with the increasing current density, which was induced by mass transport limitation and IR drop increase [42]. Clearly, compared to specific capacitance delivered at 2 Ag^{-1}, the electrode displays an excellent capacity retention rate of 74.9% after tenfold current density increment, which implies its potential for high rate application. The specific capacitance and rate capability is superior to the most results of NCS from literatures, as shown in Table S1 .The remarkable pseudocapacitive performance of CNSCS composites can be attributed to the following two factors. Firstly, the synergistic effect of nickel and cobalt ions leads to high specific capacitance. Secondly, the special 3D architecture and high porosity enable the electrolyte to penetrate easily into core region along with richer redox active sites for Faradic reactions. Moreover, the electrochemical

performance of $CoNi_2S_4$ is shown in Fig. S2. From the GCD curves, the specific capacitance value of $CoNi_2S_4$ is 1144.6 Fg^{-1} at a current density of 2 Ag^{-1} and still maintained 829.1 Fg^{-1} at 20 Ag^{-1}, which indicates its specific capacitance performance is slightly worse than CNSCS composites.

To evaluate the cycling stability of the CNSCS composites, repeated GCD measurements were performed at a large current density of 12 Ag^{-1} with a potential window of 0-0.5V, as shown in Fig. 7. There is only 2.7% decrease of the specific capacitance after 1000 consecutive cycles, indicating the excellent electrochemical stability of composites by chemical bath deposition. Moreover, the specific capacitance in the first 600 cycles tended to increase, which resulted from the full activation of CNSCS composites. The Coulombic efficiency increased from 92.7% in 100th cycles to 98.1% in 1000th cycles, which suggests excellent Coulombic efficiency.

In addition, from the pointview of practical application, the response of supercapacitors under various temperatures is important. Whereas, there is limited information about this. The effect of temperature on electrochemical performance of composites was investigated by CV and GCD measurements. Fig. 8a illustrates the CV curves of CNSCS composites at different temperatures ranging from 0 to 50 °C at 20 mVs^{-1}. The maximal integral area of the CV curves increased with the increasing testing temperature, which indicates higher specific capacitance. As shown in Fig. 8b, GCD measurements were performed from 0 to 50 °C at 10 Ag^{-1}. The GCD discharging time is in accordance with the testing temperature which indicates higher temperature, higher specific capacitance. Besides, the GCD curve shapes keep undistorted. The potential of redox reaction initial point is in contrast to the testing temperature, which means higher temperature, higher ions transport rate. The specific capacitance of CNSCS composites at different temperatures can be calculated to be 962.5, 987.5, 1030.4, 1066.9, 1115.4, 1180.9 Fg^{-1} corresponding to testing temperature of 0, 10, 20, 30, 40 and 50°C at 10 Ag^{-1}, respectively. Compared to 20 °C, the degradation of specific capacitance at 0°C is only 6.5% and the specific

capacitance at 50 °C only increases 14.6%, which indicates the stable performance of electrode in a wide temperature range.

4. Conclusions

In summary, CNSCS composites were successfully synthesized by a facile chemical bath deposition strategy. Owing to the large specific surface area (57.9 m^2/g), appropriate pore size distribution, special 3D architecture and synergistic effect of Co/Ni ions, CNSCS delivered high specific capacitance of 1183.3 Fg^{-1} at the current density of 2 Ag^{-1} and excellent rate performance (74.9% retention with tenfold increment in current density). The electrode also exhibited outstanding cycling stability, with capacitance retention of 97.3% after 1000 cycles. In addition, the electrochemical performance of electrode kept relatively stable in a wide temperature from 0ºC to 50ºC. Considering the superior electrochemical performance of CNSCS composites, the facile and efficient chemical bath deposition might be a promising processing route for CNSCS composites scalable production.

Acknowledgments

This work was financially supported by the Science and Technology Innovation Team of Sichuan Province (No. 2015TD0003), and the Program of Science and Technology Bureau of Sichuan Province (No. 2017GZ0133).

References

[1] S.E. Moosavifard, S. Fani, M. Rahmanian, Hierarchical $CuCo_2S_4$ hollow nanoneedle arrays as novel binder-free electrodes for high-performance asymmetric supercapacitors. Chem. Commun. 52 (2016) 4517–4520.

[2] B. Mendoza-Sánchez, Y. Gogotsi, Synthesis of Two-Dimensional Materials for Capacitive Energy Storage, Adv. Mater., 28 (2016) 6104–6135.

[3] M.A. Bissett, S.D. Worrall, I.A. Kinlochb, R.A.W. Dryfe, Comparison of Two-Dimensional Transition Metal Dichalcogenides for Electrochemical Supercapacitors, Electrochim. Acta 201 (2016) 30–37.

[4] M.Cakici, K.R. Reddy, F.A. Marroquin, Advanced electrochemical energy storage supercapacitors based on the flexible carbon fiber fabric-coated with uniform coral-like MnO_2 structured electrodes, Chem. Eng. J. 309 (2017) 151–158.

[5] C.S. Dai, P.Y. Chien, J.Y. Lin, S.W. Chou, W.K. Wu, P.H. Li, K.Y. Wu, T.W. Lin, Hierarchically Structured Ni_3S_2/Carbon Nanotube Composites as High Performance Cathode Materials for Asymmetric Supercapacitors, ACS Appl. Mater. Interfaces 5 (2013) 12168−12174.

[6] S. Vijayakumar, S. Lee, K. Ryu, Hierarchical $CuCo_2O_4$ nanobelts as a supercapacitor electrode with high areal and specific capacitance, Electrochim. Acta 182 (2015) 979–986.

[7] P. Wen, M. Fan, D. Yang, Y. Wang, H. Cheng, J. Wang, An asymmetric supercapacitor with ultrahigh energy density based on nickel cobalt sulfide nanocluster anchoring multi-wall carbon nanotubes hybrid, J. Power Sources 320 (2016) 28–36.

[8] R. Li, S. Wang, J. Wang, Z. Huang, Ni_3S_2@CoS core–shell nano-triangular pyramid arrays on Ni foam for high-performance supercapacitors, Phys.Chem.Chem.Phys. 17 (2015) 16434–16442.

[9] D. S. Achilleos, T. A. Hatton, Surface design and engineering of hierarchical hybrid nanostructures for asymmetric supercapacitors with improved electrochemical performance, J. Colloid Interface Sci. 447 (2015) 282–301.

[10] Y. An, Z. Hu, B. Guo, N. An, Y. Zhang, Z. Li, Y. Yang, H. Wu, Electrodeposition of honeycomb-shaped $NiCo_2O_4$ on carbon cloth as binder-free electrode for asymmetric electrochemical capacitor with high energy density, RSC Adv. 6 (2016) 37562–37573.

[11] J.J. Li, Y.X. Hu, M.C. Liu, L.B. Kong, Y.M. Hu, W. Han, Y.C. Luo, L. Kang, Mechanical alloying synthesis of Ni_3S_2 nanoparticles as electrode material for pseudocapacitor with excellent performances, J. Alloy Compd. 656 (2016) 138–145.

[12] C. Zhang, Q. Chen, H. Zhan, Supercapacitors Based on Reduced Graphene Oxide Nanofibers Supported $Ni(OH)_2$ Nanoplates with Enhanced Electrochemical Performance, ACS Appl. Mater. Interfaces 8 (2016) 22977–22987.

[13] H. Wan, J. Jiang, J. Yu, K. Xu, L. Miao, L. Zhang, H. Chen, Y. Ruan, $NiCo_2S_4$ porous nanotubes synthesis via sacrificial templates: high-performance electrode materials of supercapacitors, CrystEngComm 15 (2013) 7649–7651.

[14] A. González, E. Goikolea, J.A. Barrena, R. Mysyk, Review on supercapacitors: Technologies and materials, Renew Sust. Energy Rev. 58 (2016) 1189–1206.

[15] T. Wang, Q. Le, G. Zhang, S. Zhu, B. Guan, J. Zhang, S. Xing, Y. Zhang, Facile preparation and sulfidation analysis for activated multiparous carbon@$NiCo_2S_4$ nanostructure with enhanced supercapacitive properties. Electrochim. Acta 211 (2016) 627–635.

[16] Y. Zhao, C.A. Wang,Nano-network MnO_2/polyaniline composites with enhanced electrochemical properties for supercapacitors. Mater. Design 97 (2016) 512–518.

[17] J. Hu, M. Li, F. Lv, M. Yang, P. Tao Y. Tang, H. Liu, Z. Lu, Heterogeneous $NiCo_2O_4$@polypyrrole core/sheath nanowire arrays on Ni foam for high performance supercapacitors. J. Power Sources 294 (2015) 120–127.

[18] H. Chen, J. Jiang, L. Zhang, H. Wan, T. Qi, D. Xia, Highly conductive $NiCo_2S_4$ urchin-like nanostructures for high-rate pseudocapacitors, Nanoscale 5 (2013) 8879–8883.

[19] S. Chen, H. Chen, M. Fan, C. Li, K. Shu, Sea urchin-like Ni–Co sulfides with different Ni to Co ratios for superior electrochemical performance, J. Sol-Gel Sci. Technol. 80 (2016) 119–125.

[20] S. Chen, J. Wu, R. Zhou, Y. Chen, Y. Song, L. Wang, Controllable growth of $NiCo_2O_4$ nanoarrays on carbon fiber cloth and its anodic performance for lithium-ion batteries, RSC Adv. 5 (2015) 104433–104440.

[21] J.Y. Li, S.W. Chou, Highly transparent $NiCo_2S_4$ thin film as an effective catalyst toward triiodide reduction in dye-sensitized solar cells, Electrochem. Commun. 37 (2013) 11–14.

[22] M. Yu, J. Chen, Y. Ma, J. Zhang, J. Liu, S. Li, J. An, Hydrothermal synthesis of $NiCo_2O_4$ nanowires/nitrogen-doped graphene for high-performance supercapacitor, Appl. Surf. Sci. 314 (2014) 1000–1006.

[23] J. Pu, F. Cui, S. Chu, T. Wang, E. Sheng, Z. Wang, Preparation and Electrochemical Characterization of Hollow Hexagonal $NiCo_2S_4$ Nanoplates as Pseudocapacitor Materials. ACS Sustainable Chem. Eng. 2 (2014) 809−815.

[24] L. Lin, J. Liu, T. Liu, J. Hao, K. Ji, R. Sun, W. Zeng, Z. Wang, Growth-controlled $NiCo_2S_4$ nanosheet arrays with self-decorated nanoneedles for high-performance pseudocapacitors, J. Mater. Chem. A 3 (2015) 17652–17658.

[25] Y. Zhu, X. Ji, Z. Wu, Y. Liu, $NiCo_2S_4$ hollow microsphere decorate by acetylene black for high-performance asymmetric supercapacitor, Electrochimi. Acta 186 (2015) 562–571.

[26] J. Zhao, Z. Li , M. Zhang , A. Meng , Q. Li, Vertically cross-linked and porous $CoNi_2S_4$ nanosheets-decorated SiC nanowires with exceptional capacitive performance as a free-standing electrode for asymmetric supercapacitors, J. Power Sources 332 (2016) 355–365.

[27] J. Shen, X. Xu, P. Dong, Z. Zhang, R. Baines, J. Ji, Y. Pei, M. Ye, Design and synthesis of three-dimensional needle-like $CoNi_2S_4$/CNT/graphene nanocomposite with improved electrochemical properties. Ceram. Int. 42 (2016) 8120–8127.

[28] X. Li, Q. Li, Y. Wu, M. Rui, H. Zeng, Two-Dimensional, Porous Nickel−Cobalt Sulfide for High-Performance Asymmetric Supercapacitors. ACS Appl. Mater. Interfaces 7 (2015) 19316–19323.

[29] W. Chen, C. Xia, H. N. Alshareef, One-Step Electrodeposited Nickel Cobalt Sulfide Nanosheet Arrays for High-Performance Asymmetric Supercapacitors, ACS Nano 8 (2014) 9531–9541.

[30] S. S. Karade, D. P. Dubal, B, R. Sankapal, MoS_2 ultrathin nanoflakes for high performance supercapacitors: room temperature chemical bath deposition (CBD), RSC Adv. 6 (2016) 39159–39165.

[31] Y. Hu, H. Zhu, J. Wang, Z. Chen, Synthesis of layered birnessite-type manganese oxide thin films on plastic substrates by chemical bath deposition for flexible transparent supercapacitors, J. Alloy Compd. 509 (2011) 10234–10240.

[32] J. Pu, Z. Wang, K. Wu, N. Yu, E. Sheng, Co_9S_8 nanotube arrays supported on nickel foam for high-performance supercapacitors, Phys.Chem.Chem.Phys. 16 (2014) 785–791.

[33] X. Mao, Z. Wang, W. Kong, W. Wang, Nickel foam supported hierarchical Co_9S_8 nanostructures for asymmetric supercapacitors, New J. Chem. 41 (2017) 1142–1148.

[34] J.G. Wang, D. Jin, R. Zhou, C. Shen, K. Xie, B. Wei, One-step synthesis of $NiCo_2S_4$ ultrathin nanosheets on conductive substrates as advanced electrodes for high-efficient energy storage, J. Power Sources 306 (2016) 100–106.

[35] H. Chen, J. Jiang, Y. Zhao, L. Zhang, D. Guo, D. Xia, One-pot synthesis of porous nickel cobalt sulphides: tuning the composition for superior pseudocapacitance, J. Mater. Chem. A 3 (2015)428–437.

[36] D. Li, Y. Gong, C. Pan, Facile synthesis of hybrid CNTs/ $NiCo_2S_4$ composite for high performance supercapacitors. Sci. Rep. 6(2016) 29788.

[37] Z. Yang, X. Zhu, K. Wang, G. Ma, H. Cheng, F. Xu, Preparation of $NiCo_2S_4$ flaky arrays on Ni foam as binder-free supercapacitor electrode, Appl. Surf. Sci. 347 (2015) 690–695.

[38] Z. Gao, W. Yang, J. Wang, N. Song, X. Li, Flexible all-solid-state hierarchical $NiCo_2O_4$/porous graphene paper asymmetric supercapacitors with an exceptional combination of electrochemical properties, Nano Energy 13 (2015) 306–317.

[39] Y. Zhu, Z. Wu, M. Jing, X. Yang, W. Song, X. Ji, Mesoporous $NiCo_2S_4$ nanoparticles as high-performance electrode materials for supercapacitors, J. Power Sources 273 (2015) 584–590.

[40] Z. Wu, X. Pu, X. Ji, Y. Zhu, M. Jing, Q. Chen. F. Jiao, High Energy Density Asymmetric Supercapacitors From Mesoporous $NiCo_2S_4$ Nanosheets, Electrochim. Acta 174 (2015) 238–245.

[41] P. Simon, Y. Gogotsi, B. Dunn. Where Do Batteries End and Supercapacitors Begin, Science 343 (2014) 1210–1211.

[42] X. Xiong, G. Waller, D. Ding, D. Chen, B. Rainwater, B. Zhao, Z. Wang, M. Liu. Controlled synthesis of $NiCo_2S_4$ nanostructured arrays on carbon fiber paper for high-performance pseudocapacitors, Nano Energy 16 (2015) 71–80.

[43] W. Du, Z. Zhu, Y. Wang, J. Liu, W. Yang, X. Qian, H. Pang, One-step synthesis of $CoNi_2S_4$ nanoparticles for supercapacitor electrodes, RSC Adv. 4 (2014) 6998–7002.

[44] Y. Xiao, D. Su, X. Wang, L. Zhou, S. Wu, F. Li, S. Fang, In suit growth of ultradispersed $NiCo_2S_4$ nanoparticles on graphene for asymmetric supercapacitors, Electrochim. Acta 176 (2015) 44–50.

.

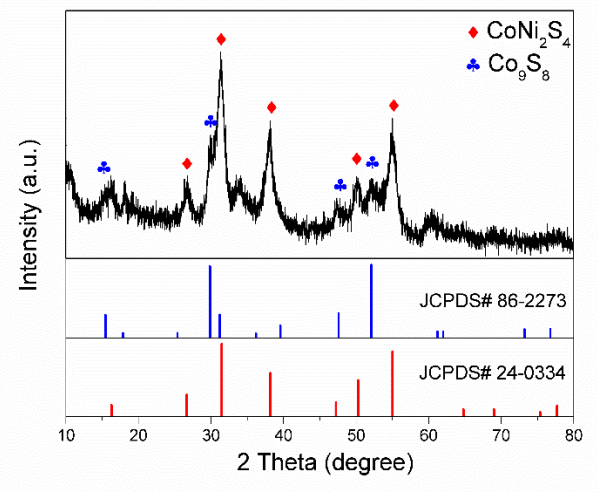

Fig. 1 XRD pattern of the as-prepared products.

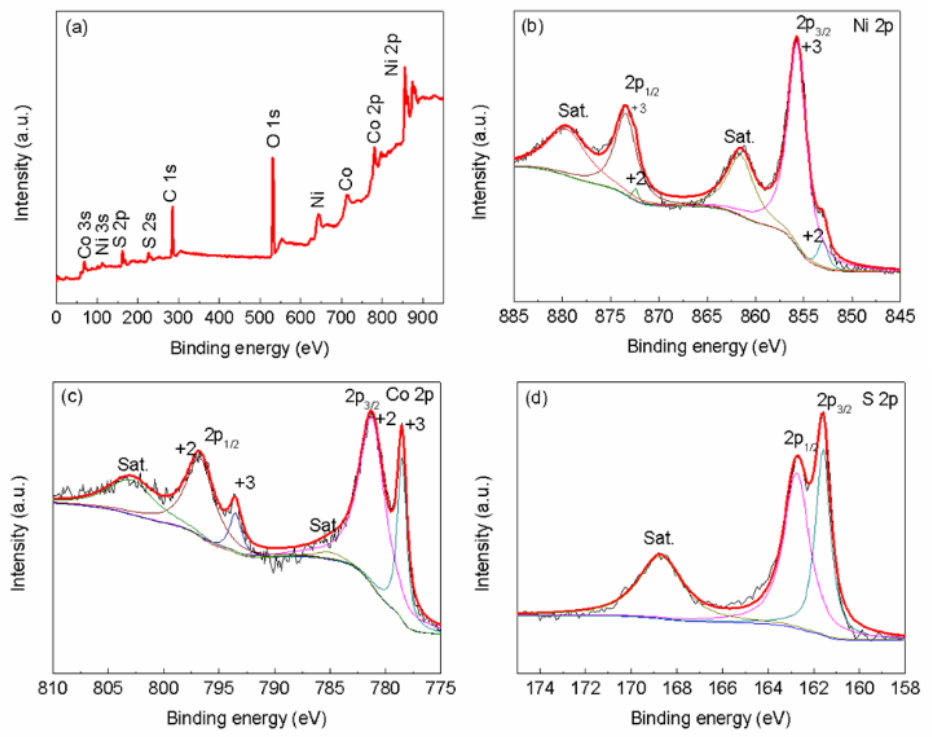

Fig. 2 XPS spectra of the CNSCS composites, (a) survey spectrum; (b) Ni 2p; (c) Co 2p and (d) S 2p.

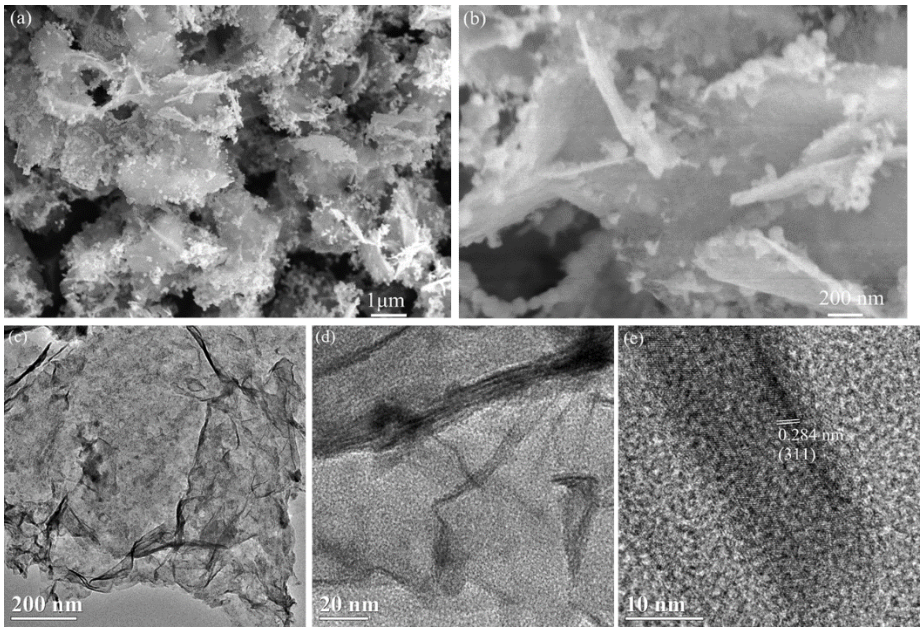

Fig. 3 SEM (a, b) and TEM (c, d and e) images of CNSCS composites.

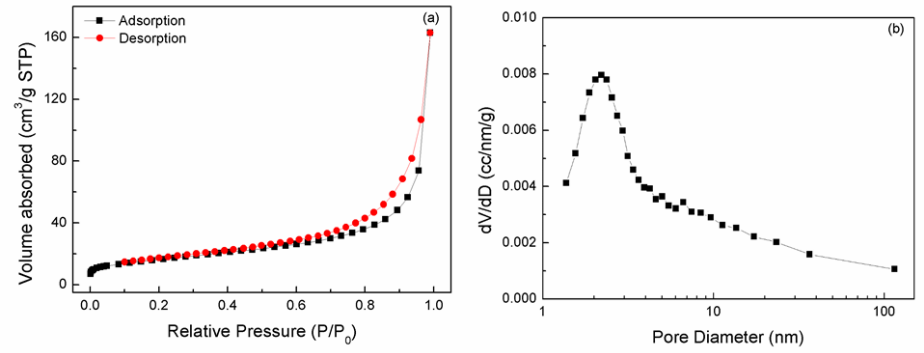

Fig.4. (a) Nitrogen adsorption-desorption isotherm of CNSCS composites; (b) pore size distribution of CNSCS composites.

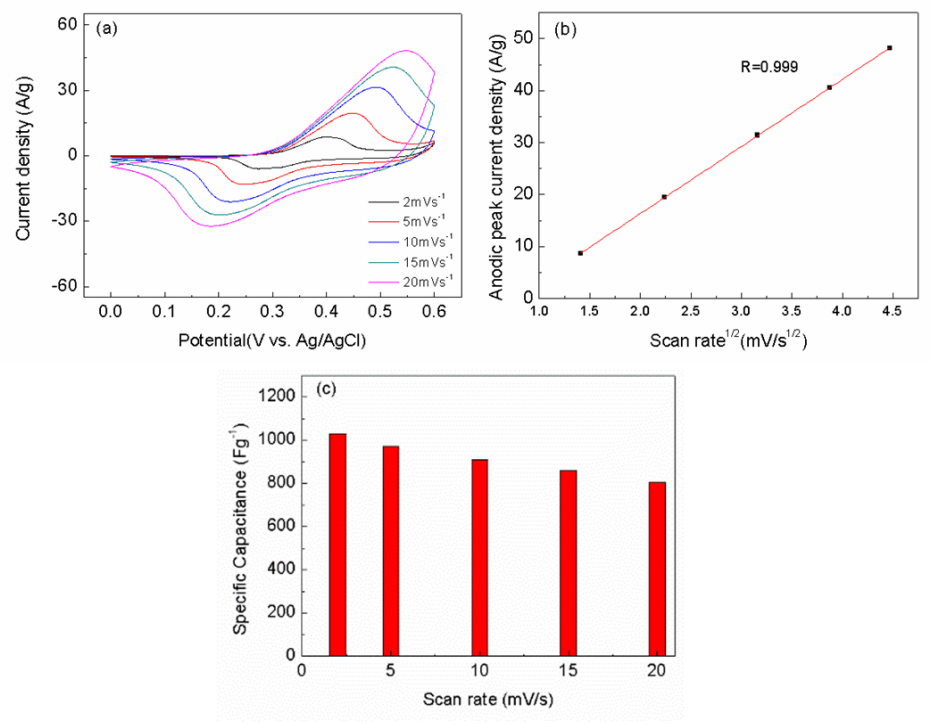

Fig.5. (a) CV curves of CNSCS composites at different scan rates; (b) the anodic peak current *vs*. the square root of scan rate of CNSCS composites; (c) the specific capacitance of CNSCS composites at different scan rates.

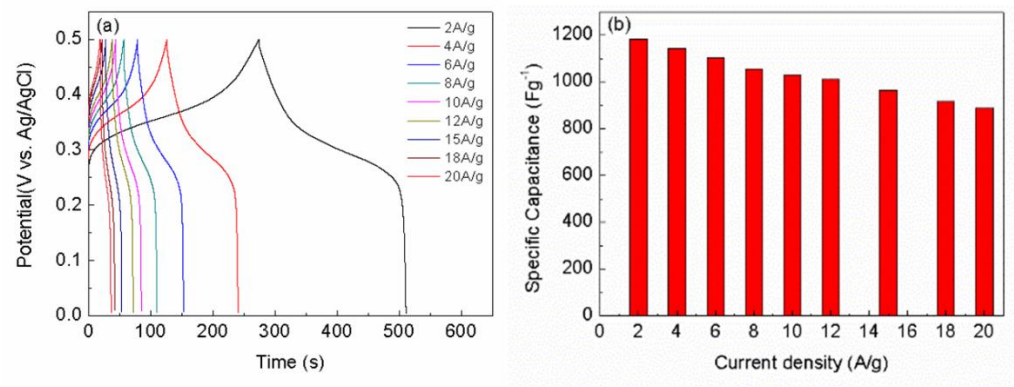

Fig. 6 GCD curves (a) and the specific capacitance (b) of CNSCS composites at different current densities.

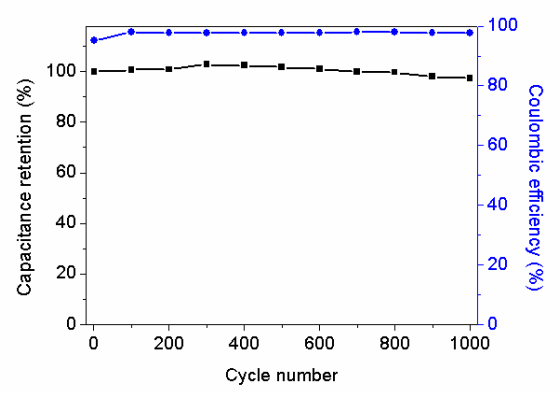

Fig. 7 Capacitance retention and Coulombic efficiency of CNSCS composites at the current density 12 Ag^{-1}.

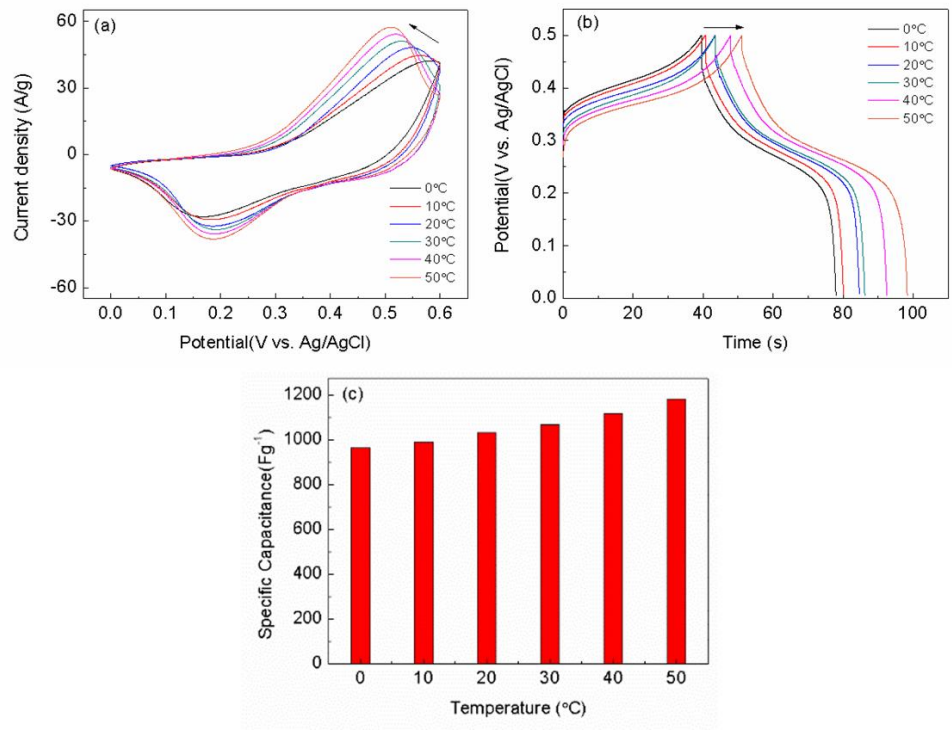

Fig. 8 CV curves (a), GCD curves (b) and specific capacitance (c) of CNSCS composites at different temperatures.